nature communications

Article

https://doi.org/10.1038/s41467-025-60915-x

Stable ultrafast graphene hot-electron source on optical fiber

Received: 13 December 2024

Accepted: 9 June 2025

Published online: 01 July 2025

Check for updates

Guangjie Yao[1,2,11], Hao Hong[1,3,11] ✉, Xu Zhou[4,11], Kaifeng Lin[1,2,11], Huazhan Liu[1], Yilong You[1], Chang Liu[1], Ke Chen[5], Chi Li[5], Jianbo Yin[6], Zhujun Wang[7], Xuewen Fu[8], Qing Dai[5] ✉, Dapeng Yu[1,9] ✉ & Kaihui Liu[1,10] ✉

A stable and durable ultrafast electron source is highly desirable for sophisticated vacuum electron technologies. However, free-space excitations based on ultrahigh-power or deep-ultraviolet pulsed lasers usually cause cathode material damage and mechanical vibration even under ultrahigh vacuum. In this work, we present a compact ultrafast electron source consisting of graphene integrated on an optical fiber, taking advantage of the ultrafast hot-electron emission from graphene and well-defined single-mode excitation from the optical fiber. With mild excitation (~1 GW/cm^2, infrared laser), an ultrashort electron pulse (width of ~ 80 fs) with high stability (fluctuation ≤±0.5% in 8 hours) and longevity (T_{90} > 500 hours) can be generated even under relatively high ambient pressure (up to 100 Pa). This compact source has been facilely integrated into a commercial electron microscope for time-resolved imaging and spectroscopy. Our graphene optical fiber-based ultrafast electron source offers a promising solution to support the development of vacuum electron instruments.

An ultrafast electron microscope system enables monitoring of microscopic evolution at high spatial and temporal resolutions through ultrafast electron diffraction, imaging, energy loss spectroscopy, and cathodoluminescence (CL)[1–5]. The characterization resolution and functionality of the system are directly determined by the performance of the ultrafast electron source[6–9]. Generally, the pulsed electron emission from a photocathode (typically made of metallic materials such as gold, tungsten or LaB_6 or low-dimensional materials such as carbon nanotubes or fullerene) is driven by mechanisms of multiphoton emission, optical field emission or the photoelectric effect under ultrafast laser pumping[10–14]. For multiphoton emission and optical field emission, a very intense laser (~100 GW/cm^2) is required, which may often cause distinct damage (atom evaporation, local melting, oxidization, etc.) to the cathode materials[15] and requires an ultrahigh vacuum environment (~10^{-7} Pa). For the photoelectric effect, single-photon excitation with a low-intensity laser is applicable, but the ultraviolet pump light (photon energy of typically above 3.6–5 eV) complicates the laser system and is more likely to cause ionization and damage to the cathode materials[16]. These harsh operating conditions directly reduce the stability and lifetime of the

[1]State Key Lab for Mesoscopic Physics and Frontiers Science Center for Nano-optoelectronics, School of Physics, Peking University, Beijing, China. [2]Academy for Advanced Interdisciplinary Studies, Peking University, Beijing, China. [3]Interdisciplinary Institute of Light-Element Quantum Materials and Research Center for Light-Element Advanced Materials, Peking University, Beijing, China. [4]Guangdong Provincial Key Laboratory of Quantum Engineering and Quantum Materials, School of Physics, South China Normal University, Guangzhou, China. [5]Division of Nanophotonics, National Center for Nanoscience and Technology, Beijing, China. [6]State Key Laboratory of Photonics and Communications, School of Electronics, Peking University, Beijing, China. [7]School of Physical Science and Technology, Shanghai Tech University, Shanghai, China. [8]Ultrafast Electron Microscopy Laboratory, School of Physics, Nankai University, Tianjin, China. [9]Shenzhen Institute for Quantum Science and Engineering, Shenzhen, China. [10]International Centre for Quantum Materials, Collaborative Innovation Centre of Quantum Matter, Peking University, Beijing, China. [11]These authors contributed equally: Guangjie Yao, Hao Hong, Xu Zhou, Kaifeng Lin. ✉e-mail: haohong@pku.edu.cn; daiq@nanoctr.cn; yudp@sustech.edu.cn; khliu@pku.edu.cn

photocathode and increase the complexity of utilizing ultrafast electron sources. Moreover, most of the available ultrafast electron sources suffer from an unavoidable time-dependent beam current decay under the ultrafast laser excitation and have to reflash and re-focus after each operation period (usually 4–6 hours)[17,18], causing the low operation efficiency and unstable data quality of the ultrafast electron microscopy. Therefore, despite the extensive progress and successful application of ultrafast electron sources in recent decades, there is still a pressing need to explore photocathode materials and driving mechanisms for a stable ultrafast electron source that can broaden its applications.

Graphene is a promising material for photoemission due to its unique hot-carrier dynamics. After photoexcitation, electrons in graphene undergo ultrafast thermalization and energy up-conversion driven by strong electron–electron scattering[19–25], which is determined to be much more efficient than that of conventional metals[26]. The hot carriers are distributed over the entire Dirac energy band, with a quasi-equilibrium temperature of a few thousand Kelvins on an ultrashort time scale of ~30 fs. These unique ultrafast dynamic processes make graphene appealing for diverse photonic and optoelectronic devices[27–32]. In principle, the hot carriers in graphene also have the possibility of overcoming the work function and escaping into the vacuum for electron emission in an ultrafast way[33].

Potentially, the ultrafast hot-electron emission from graphene has the following advantages: (i) the pulsed laser mainly heats the electrons, with the lattice mostly remaining cool (typically lower than 400 K)[22], allowing graphene to serve as an ultrastable photocathode for a long operation time without the need for an strictly high vacuum; (ii) the electron thermalization (~30 fs) and cooling (~1 ps) are transient processes, resulting in an ultrashort electron pulse width; and (iii) the hot-carrier distribution strongly depends on the pump fluence rather than the pump photon energy, so a relatively low-power near-infrared laser can efficiently heat hot carriers to produce a large photoemission flux[26]. Thus, graphene holds great potential as an ultrafast electron source with great stability by exploiting ultrafast and efficient hot-carrier thermalization. Recently, static thermionic electron emission from graphene under direct laser or electric heating has been observed[34,35], utilizing strong carbon–carbon bonds and ultralow defect densities for thermal stability. However, hot-electron photoemission from graphene for ultrafast electron source usage still needs to be fully explored.

Here, we present a stable ultrafast hot-electron source by integrating graphene on the end face of a single-mode optical fiber. In addition to their good integrability[36,37], we demonstrate that optical fibers can be elaborately used to further augment the stability, as they provide stable and tight focusing of a well-defined Gaussian optical mode for driving electron emission. By exploiting the hot-carrier thermalization mechanism and the unique architecture of optical fiber integration, we show that our graphene ultrafast hot-electron source exhibits state-of-the-art high performance and merits of superior stabilities, encompassing operational fluctuations, durability, cyclability and pressure tolerance.

Results and discussion

Photo-induced graphene hot-electron emitter on optical fiber

In our experiment, we fabricate an optical fiber-integrated graphene hot-electron source (Fig. 1a) by transferring mechanically exfoliated graphene onto the end face of a single-mode optical fiber (Fig. 1b) (see Methods and Supplementary Fig. 1 for fabrication details). Graphene is grounded via contact with a pre-deposited gold pattern, and an opposite anode (~170 μm from cathode) is positively biased to collect vacuum electrons emitted from graphene. The pump laser (photon energy of 0.8 eV, pulse width of ~250 fs, repetition rate of 80 MHz, if not otherwise specified) is directly coupled into the other end of the optical fiber (mode field diameter of ~10 μm) and tightly illuminates the graphene. During the experiments, we record the ultrafast photoluminescence (PL) and photoemission current from graphene by means of a spectrometer and a source meter, respectively (see Methods for details). The ultrafast PL spectrum exhibits a broadband curve ranging from the near-infrared to visible region, which stems from the blackbody radiation of hot carriers in graphene (Fig. 1c) and can be well fitted with Planck's law (solid fitting lines)[19,20]. By extracting the temperature parameter from the spectra, we obtain an excitation power-dependent electron temperature (T_e), as shown in Fig. 1d. The electron temperature monotonically increases with excitation power and reaches more than 2500 K at 35 mW excitation. Simultaneously, we find a significant current between the graphene cathode and the opposite anode, indicating the successful detection of photoemission from graphene. The photoemission current depends on both the bias voltage (V_b) and excitation power. It slowly increases with bias voltage according to a sublinear relation (Fig. 1e, which can be described by Longo equation of thermionic emission[38] as shown in Supplementary Fig. 2) and exhibits a high-order nonlinear dependence on the laser excitation power (power dependence order of ~4.8).

The photoemission behavior of our graphene photocathode is quite different from that of conventional static electric field emission, where the ultrafast electron emission is driven by the mechanism of multiphoton emission or the photoelectric effect. In the case of electric field-driven electron emission, the Fowler–Nordheim equation describes a drastic increase in current with applied voltage[39], which contrasts with the small electric field (<0.1 V/μm) and slow-varying current shown in Fig. 1e. For a photocathode working in the multiphoton emission regime, the product of the photon energy ($h\nu$ =0.8 eV) and power dependence order ($n\approx4.8$) should exceed the material work function (Fig. 1f). However, the calculated value of $n \cdot h\nu$ =3.8 eV is far below the work function of graphene (~4.5 eV)[27,35] for photoemission. Moreover, photoexcitation at 1.55 eV yields a similar value of $n\approx4.9$ as that at 0.8 eV, which deviates from the scenarios of multiphoton emission and the photoelectric effect (Supplementary Fig. 3 and Supplementary Fig. 4).

The high electron temperature suggests the mechanism of hot-electron emission in graphene. Figure 1g shows the photoemission current as a function of the electron temperature. The current (I) drastically increases with temperature, which can be well described by the Richardson–Dushman law as

$$I = CT_e^2 \exp\left(-\frac{\phi}{k_B T_e}\right), \tag{1}$$

where C is a constant related to the emission geometry, k_B is the Boltzmann constant, T_e is the electron temperature, and ϕ is the work function of graphene. $\ln(I/{T_e}^2)$ versus $1/T_e$ demonstrates a high degree of linearity, as shown in Fig. 1h, confirming the occurrence of a thermionic electron emission mechanism.

Temporal characterization of electron pulse

The mechanism of hot-electron emission with transient thermalization and cooling of hot carriers enables graphene to generate an ultrafast electron pulse. Figure 2a, b shows the calculated Fermi-Dirac distribution and population density distribution in graphene as a function of energy at different electron temperatures. As the temperature increases, electrons with energy above the work function ϕ will escape from graphene into the vacuum and contribute to electron emission. Thus, we can obtain temporal information on the blackbody radiation and electron emission current based on the temperature evolution of hot carriers after photoexcitation (Supplementary Note 1). Theoretically, the hot carriers follow a two-temperature model (Fig. 2c)[20]. After excitation, the intraband and interband carrier scattering impel photoexcited electrons and holes to thermalize at an equilibrium temperature (T_e) and extend their distribution throughout the whole

https://doi.org/10.1038/s41467-025-60915-x

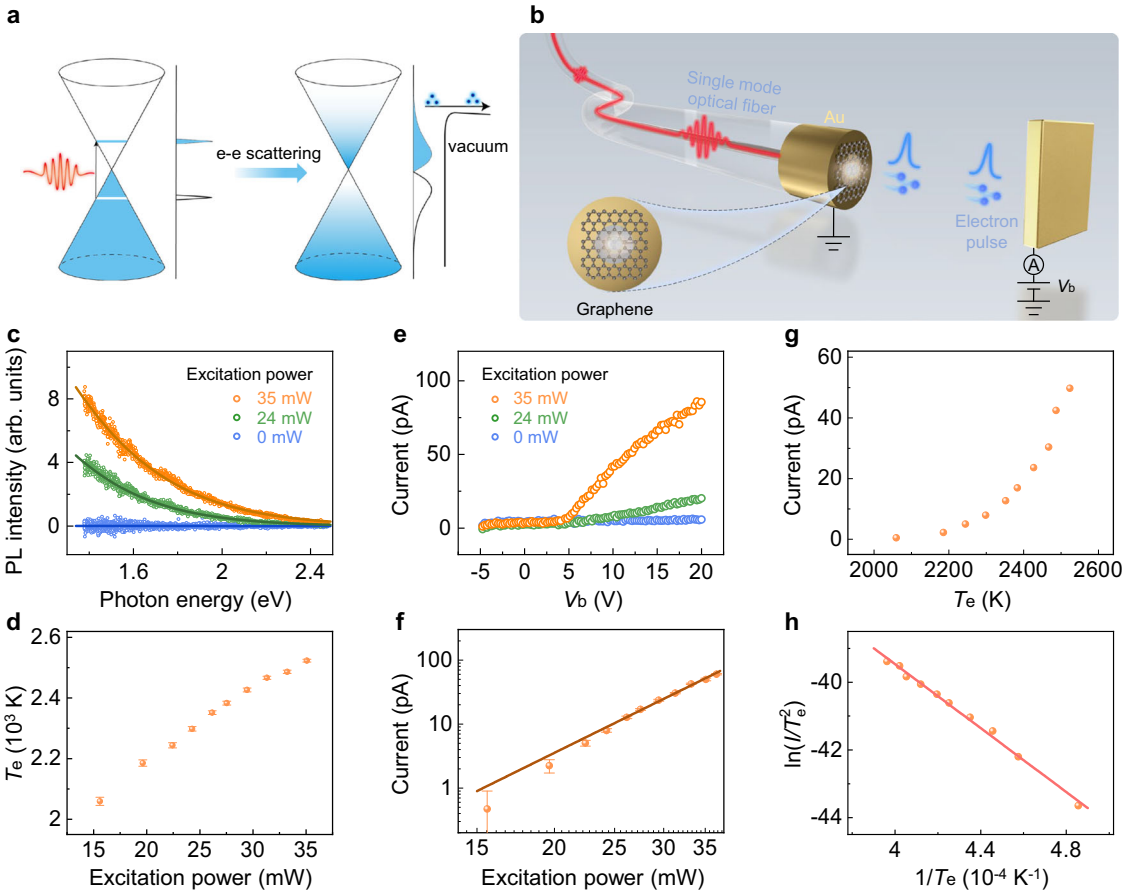

Fig. 1 | Optical fiber-integrated graphene ultrafast hot-electron emitter. **a** Mechanism of hot-electron emission from graphene after pulsed laser excitation. The carrier distribution evolves from discrete energy levels to quasi-equilibrium thermalization, which is driven by strong electron–electron scattering. The thermalized hot electrons with energies above the graphene work function escape into the vacuum for electron emission. **b** Illustration of the optical fiber-integrated graphene ultrafast hot-electron source. Graphene is capped onto the end face of an optical fiber and grounded via a pre-deposited gold pattern. Under pulsed laser excitation coupled into the optical fiber, graphene exhibits ultrafast photoluminescence (PL) and photoemission. **c** Excitation power-dependent ultrafast PL spectra (circles) of optical fiber-integrated graphene. The spectra can be fitted with Planck's law of blackbody radiation (solid lines). **d** Derived electron temperature (T_e) as a function of excitation power. Error bars are from fitting standard error. **e** Collected photoemission current as a function of bias voltage (V_b) under different excitation powers. The current sublinearly increases with V_b. **f** Excitation power-dependent photoemission current at $V_b = 10$ V. The current nonlinearly increases with increasing excitation power, with a fitting slope of ~4.8. The error bars are from the standard deviation across about 100 points. **g** Collected photoemission current as a function of hot-electron temperature. **h** Richardson–Dushman plot of the data in (**g**). The linear fitting yields a work function of 4.1 eV, which is very close to that of suspended graphene. All the acquired data are obtained under 1560 nm pulsed laser excitation with a single-mode optical fiber.

energy band on a timescale of ~30 fs[20,22]. Then, the hot carriers experience further cooling and relaxation via scattering with optical phonons located in **Γ** and **K** points of Brillouin zone[40,41] (with energy scale of ~160–200 meV, temperature labeled as T_{ph}). Finally, both electron and optical phonon system loss energy to the low-energy acoustic phonon system and cool down (Fig. 2c). During the transient thermalization process (electron transport time within graphene is neglected due to the atomic-scale thickness), the time-resolved electron emission can be derived from the Richardson–Dushman law (Fig. 2d). The electron pulse has a pulse width of ~85 fs, with a negligible thermal lag effect (Supplementary Fig. 5).

Experimentally, we employ two-pulse autocorrelation measurements (Supplementary Fig. 6) to obtain temporal information about the ultrafast PL (Supplementary Fig. 7) and electron emission at the same time[19,20]. As shown in Fig. 2e, the time-resolved electron emission current exhibits a dynamic lifetime of ~60 fs. Because the electron transit time to the surface can be negligible due to graphene's atomic-scale thickness, this 60 fs lifetime corresponds to a pulse width of ~80 fs (Supplementary Fig. 8)[27]. Moreover, the electron dynamic lifetime is nearly independent of excitation power (Supplementary Fig. 9). We note that the ~60 fs lifetime is limited by the width of the laser pulse (~180 fs) used in our optical fiber. We further test a graphene electron emission source fabricated on a Si/SiO_2 substrate under ~40 fs near-infrared (~1.55 eV) laser pumping and find an ~25 fs electron dynamic lifetime (Supplementary Fig. 10). The compressed dynamic lifetime in electron emission is attributed to the high nonlinearity of the carrier thermalization, which agrees well with our theory (Fig. 2f).

Efficiency and stability of graphene ultrafast electron source

The unique ultrafast hot-electron emission mechanism and the optical fiber-integrated architecture endow graphene with excellent photoemission efficiency and stability. Due to the effective hot-carrier thermalization[24,26], the quantum efficiency (defined by collected electron flux over incident photon flux) of hot-electron emission is determined to be ~10^{-9} at 2.2 GW/cm² for graphene, which is several orders of magnitude greater than that of traditional multiphoton or optical field emission under the same low pump intensity (Fig. 3a). The utilization of a low-intensity near-infrared laser and a weak electric field (<0.1 V/μm) for hot-electron emission in graphene potentially mitigates the effects of ion back-bombardment, gas adsorption and local melting. Crucially, the pulsed laser only heats the carriers, while the lattice mostly remains cool[20], thus preventing thermal evaporation of

https://doi.org/10.1038/s41467-025-60915-x

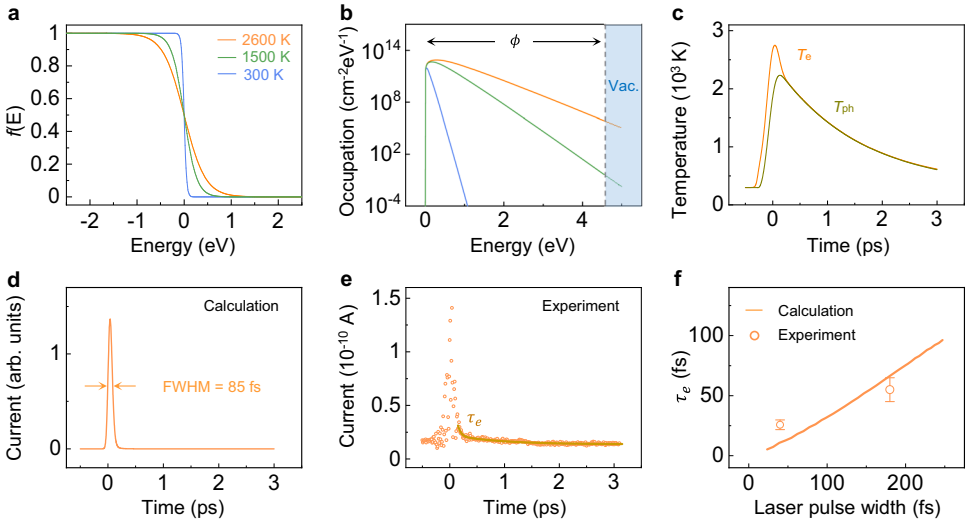

Fig. 2 | Temporal information of ultrafast hot-electron emission from graphene. a Fermi-Dirac distribution (f(E)) at different electron temperatures. **b** Electron occupation as a function of energy above the Dirac point at different temperatures. Electrons with energies above the work function (ϕ) can escape from graphene for electron emission. **c** Temperature evolution after ~180 fs pulsed laser excitation. The electron temperature (T_e) increases within 100 fs time scale and quickly reaches equilibrium with phonons (T_{ph}). **d** Calculated ultrafast hot-electron emission pulse width in graphene. Based on the evolution of the hot-electron temperature, the time-resolved photoemission current can be calculated to have a full width at half maximum (FWHM) of ~85 fs. **e** Time-resolved autocorrelation of the photoemission current in graphene. Under pulsed laser excitation (~180 fs, 800 nm, 18 mW), two dynamic lifetimes (~60 fs and ~800 fs, faster one is defined as τ_e) can be derived from the decay part of the intensity behavior by exponential fitting. **f** Derived electron emission lifetimes for different excitation pulse widths. The test data with ~180 fs and ~40 fs excitations well matches the calculations. The error bars are from autocorrelation decay fitting standard error. Data in (**e**) together with derived data (180 fs laser pulse width in (**f**)) is obtained under 800 nm excitation within optical fiber. The 40 fs excitation data point in (**f**) is obtained under 800 nm excitation via free-space focusing.

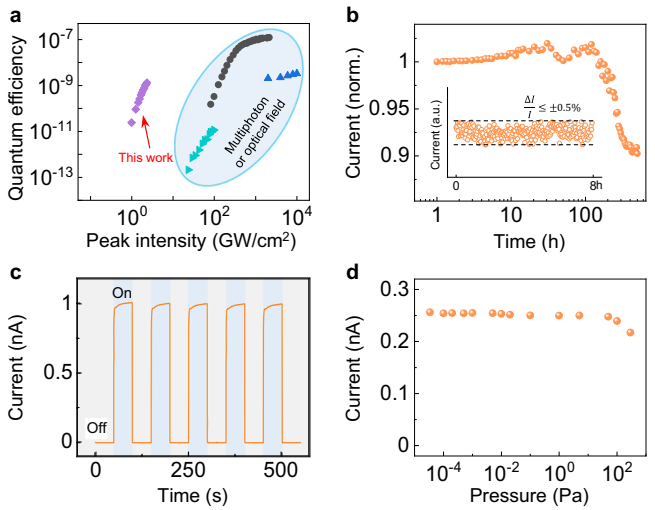

Fig. 3 | Highly efficient and stable graphene ultrafast hot-electron source. a Overview of the electron emission quantum efficiency driven by different mechanisms. Hot-electron thermalization in graphene is much more efficient than the typical multiphoton or optical field emission of metals at low peak intensities. The data in the closed circle are from previous studies[12,42,43]. **b** Operational fluctuation and durability test of the optical fiber-integrated graphene hot-electron source. The fluctuations remain within ±0.5% for 8 hours (inset), and the T_{90} lifetime is determined to be 500 hours under continuous operation. **c** Measurement of excitation laser on-off loops. The emission current remains within ±0.4% when the laser is repeatedly turned on and drops to zero when it is turned off, demonstrating a pure pulsed feature. **d** Photoemission current under various chamber pressures. The current remains almost constant below ~70 Pa. All the acquired data are obtained under 1560 nm pulsed laser excitation with single-mode optical fiber.

carbon atoms. Furthermore, our system employs a single-mode optical fiber to selectively couple the fundamental mode laser for tight-focus excitation. This strategy effectively reduces the influence of vibrations from the optical mode and focus status. Additionally, graphene's robust in-plane carbon-carbon bonding and lack of out-of-plane dangling bonds contribute to a stable electron emission surface, effectively inhibiting atom evaporation. Consequently, our graphene hot-electron source integrated with an optical fiber exhibits significant potential for stability, encompassing operational fluctuations, durability, cyclability and pressure tolerance.

To quantitatively evaluate the operational fluctuations and durability, we fix the laser excitation power and monitor the emission current over time (Fig. 3b). The fluctuations remain within ±0.5% for 8 hours (Fig. 3b inset), which should be the most stable ultrafast electron source to our knowledge (Supplementary Table 1). The continuous operation lifetime T_{90} (defined as the time at which the emission current decreases to 90% of the initial value) is determined to be ~500 hours, which is one of the highest among all the reported ultrafast electron sources. During the on–off cycling test of the laser, the emission current remains within ±0.4% when the laser is repeatedly turned on at 44 mW (Fig. 3c). When the laser is turned off, the photoemission current can be completely shut down, benefiting from the low driven static electric field (eliminating the static electric field emission in our architecture), which ensures the production of pure pulsed electrons without the interference of continuous electron signals.

Figure 3d shows the stable emission current at different working pressures. The cool lattice guarantees the reliability of the electron emission process under a poor vacuum environment. Thus, the current remains almost constant as the pressure increases from 10^{-5} Pa to 10^{1} Pa. It even has significant current under 10^{2} Pa, in contrast to the conventional ultrafast electron sources requiring ~10^{-7} Pa. This means

https://doi.org/10.1038/s41467-025-60915-x

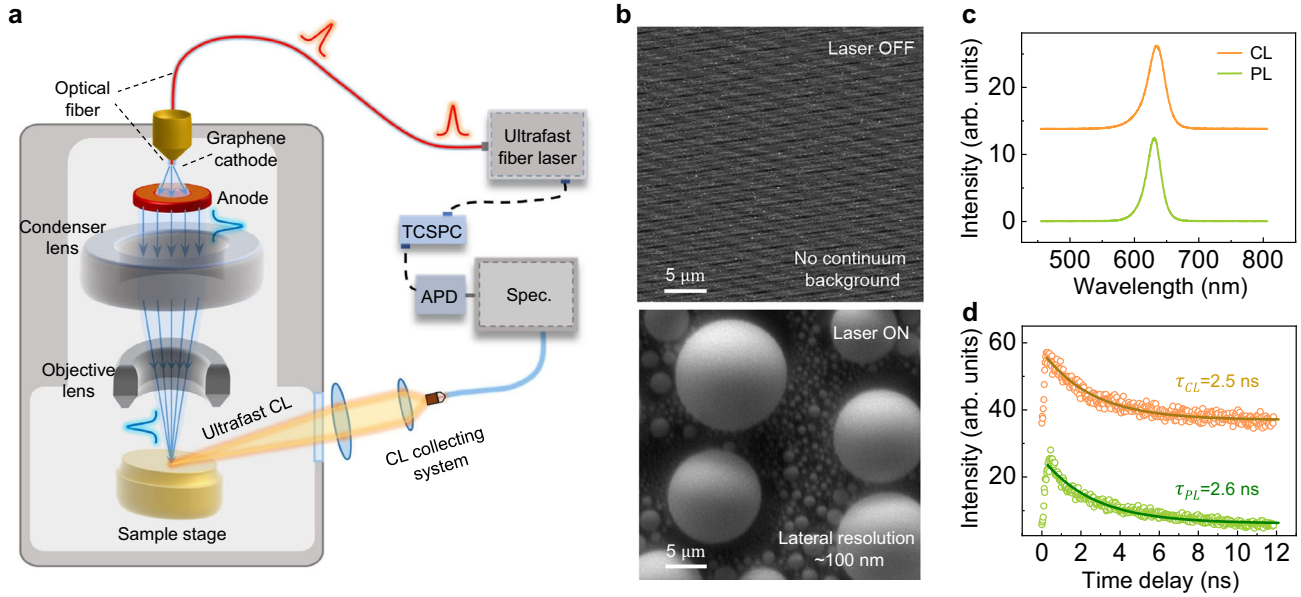

Fig. 4 | Ultrafast scanning electron microscope (SEM) based on the optical fiber-integrated graphene ultrafast hot-electron source. a Schematic diagram of our ultrafast SEM. A traditional scanning microscope body is equipped with our optical fiber-integrated graphene ultrafast hot-electron source for spatial and temporal imaging. CL: Cathodoluminescence; TCSPC: Time-correlated single-photon counting; APD: Avalanche photodiode. **b** Images obtained from the ultrafast electron microscope using a secondary electron detector. High signal-to-background ratio images can be captured when the laser is turned on, benefiting from the pure pulsed electrons from graphene. **c** CL and far-field PL spectra of CdSe/ZnS quantum dots. **d** Time-resolved CL and PL spectra (circles) of CdSe/ZnS quantum dots. The exponential decay fitting (solid lines) gives decay lifetimes of CL (τ_{CL}) and PL (τ_{PL}) of 2.5 ns and 2.6 ns, respectively. The optical excitation at 1560 nm is transmitted via optical fiber.

that an individual primary pump (i.e., scroll pump) can meet the requirements for normal operation of our ultrafast electron source. We note that the slight current decrease under high pressure is attributed to the shortened electron mean free path and gas absorption at high pressure, which can recover as the pressure decreases (Supplementary Fig. 11).

Integration on ultrafast scanning electron microscope

This kind of electron source shows state-of-the-art high performance and great integrability for equipment. The brightness properties of the source are measured (Supplementary Table 2), with a normalized root mean square emittance of 46 nm · rad (Supplementary Fig. 12), peak reduced brightness of $2.7 \times 10^4 A/(m^2 \cdot sr \cdot V)$ (Supplementary Note 2) and energy spread of FWHM = 0.5 eV (Supplementary Fig. 13). As a demonstration example, we equip the optical fiber-integrated graphene ultrafast hot-electron source on a commercial desktop scanning electron microscope (SEM) to empower the time-resolved capability (Fig. 4a). The tailormade electron gun is composed of the optical fiber-integrated graphene ultrafast hot-electron source, a Wehnelt cylinder and anode electrodes. Under laser excitation, clear images can be obtained using an Everhart-Thornley (E-T) detector (Fig. 4b bottom), showing a lateral resolution of ~100 nm (Supplementary Fig. 14). When the excitation laser is turned off, totally dark images are collected (Fig. 4b top). This high signal-to-background ratio for high-sensitivity detection benefits from the pure pulsed electrons, as characterized in Fig. 3c. Utilizing this system, we successfully characterize the CL and time-resolved CL spectra of a CdSe/ZnS quantum dot film (Fig. 4c,d), which are consistent with their far-field optical excitation PL and time-resolved PL spectra, respectively.

In summary, we present a stable ultrafast electron source based on optical fiber-integrated graphene by exploiting a hot-carrier thermalization mechanism and a unique optical fiber integration architecture. In contrast to conventional ultrafast electron sources, our fiber-integrated graphene emitter exhibits direct instrumental compatibility and maintains stable performance in low vacuum environments, under a low-intensity near-infrared laser excitation. In the future, by manipulating the optical modes of optical fibers and employing the rich properties of 2D materials for surface-state electron emission, our approach suggests a path to construct versatile ultrafast electron sources, such as electron beams with spin, orbital momentum or high coherence.

Methods

Fabrication of optical fiber-integrated graphene electron source

The fabrication is based on single-mode optical fiber (Corning SMF-28e+ at 1560 nm and YOFC CS-780 at 800 nm) and mechanically exfoliated graphene. Monolayer to few-layer graphene is prepared on the PPC (polypropylene carbonate) film by tapes, which are spin-coated on SiO_2/Si. The PPC film is peeled off and upside-down suspended, holding the wanted sample at the bottom side. A ~10 μm PMMA (polymethyl methacrylate) microsphere is first placed on the optical fiber to cover the fiber core. Then, the optical fiber is deposited with a conducting film of 5 nm Pd (adhesion layer) and 60 nm Au by electron beam evaporation. After that, the fiber is immersed in acetone to remove the PMMA microsphere, leaving the exposed fiber core. The prepared graphene sample on suspended PPC film is then transferred onto the fiber end face. After alignment and contact of the fiber core and graphene sample, graphene is released by heating to 130 °C. The residual PPC is removed by acetone.

Optical excitation and measurement setup

The excitation pulsed laser used in this work contains different types: Spectra-Physics Mai Tai oscillator (~100 fs, 80 MHz, 690–1050 nm), NPI Rainbow 1550 OEM ultrafast optical fiber laser (~80 fs, 80 MHz, 1560 nm), Coherent Vitara oscillator (~15 fs, 80 MHz, 800 nm) and Chameleon Ultra II (~140 fs, 80 MHz, 680–1080 nm). A compensating fiber (NKT HC-800) is used to compress the pulse width to about 180 fs, as it couples the 800 nm Mai Tai beam into an optical fiber. Under 1560 nm excitation, the pulse width at the graphene position is measured as ~250 fs (APE PulseCheck USB-15). Under

35 mW excitation, the peak intensity is calculated to be ~2.2 GW/cm^2 with a laser spot diameter of ~10 µm, a pulse width of ~250 fs and a repetition rate of 80 MHz. Hot-electron emission autocorrelation of the on-chip device is conducted using Vitara with a tested pulse width of ~40 fs at 800 nm. To obtain a precise ultrafast PL spectrum, the collecting system, including the collecting fiber and the spectrometer, is calibrated using the blackbody light source (Newport Oriel). The optical signal is measured by a Princeton SP2500 spectrometer. Electron energy spectrum emitted from graphene with 800 nm excitation (Chameleon Ultra II, ~180 fs at sample position) is measured in a photoemission electron microscopy (FOCUS, IS-PEEM) equipped with an imaging energy filter (IEF) type electron energy analyzer.

Electrical measurement setup

The electrical measurement system is based on a customized optical fiber test holder. Applied voltage (± 200 V maximum) and anode collecting current (0.1 fA resolution) are conducted through Keithley 2636B source meter. All the experiments are conducted at room temperature.

Ultrafast SEM imaging and spectroscopy

The ultrafast electron microscope is modified based on ZEM-15 (ZEPTOOLS). The initial tungsten thermal electron gun is replaced by an optical fiber-integrated graphene ultrafast hot-electron gun with careful alignment with the electron optical axis. The image is captured with an E-T type secondary electron detector with excitation laser at 1560 nm (NPI Rainbow 1550 OEM). CL is collected and guided to the spectrometer (Princeton SP2500) and a time-correlated single-photon counting (TCSPC) system with an avalanche photodiode detector (Picoquant, Timeharp 260).

Data availability

Relevant data supporting the key findings of this study are available within the article and the Supplementary Information file. All raw data generated during the current study are available from the corresponding authors upon request.

References

1. Williamson, S., Mourou, G. & Li, J. C. M. Time-resolved laser-induced phase transformation in aluminum. *Phys. Rev. Lett.* **52**, 2364–2367 (1984).
2. Siwick, B. J., Dwyer, J. R., Jordan, R. E. & Miller, R. J. D. An atomic-level view of melting using femtosecond electron diffraction. *Science* **302**, 1382–1385 (2003).
3. Zewail, A. H. Four-dimensional electron microscopy. *Science* **328**, 187–193 (2010).
4. Merano, M. et al. Probing carrier dynamics in nanostructures by picosecond cathodoluminescence. *Nature* **438**, 479–482 (2005).
5. Filippetto, D. et al. Ultrafast electron diffraction: Visualizing dynamic states of matter. *Rev. Mod. Phys.* **94**, 045004 (2022).
6. Aidelsburger, M., Kirchner, F. O., Krausz, F. & Baum, P. Single-electron pulses for ultrafast diffraction. *Proc. Natl Acad. Sci. USA* **107**, 19714–19719 (2010).
7. Krüger, M., Schenk, M. & Hommelhoff, P. Attosecond control of electrons emitted from a nanoscale metal tip. *Nature* **475**, 78–81 (2011).
8. Nabben, D., Kuttruff, J., Stolz, L., Ryabov, A. & Baum, P. Attosecond electron microscopy of sub-cycle optical dynamics. *Nature* **619**, 63–67 (2023).
9. Piglosiewicz, B. et al. Carrier-envelope phase effects on the strong-field photoemission of electrons from metallic nanostructures. *Nat. Photon.* **8**, 37–42 (2014).
10. Ropers, C., Solli, D. R., Schulz, C. P., Lienau, C. & Elsaesser, T. Localized multiphoton emission of femtosecond electron pulses from metal nanotips. *Phys. Rev. Lett.* **98**, 043907 (2007).
11. Damascelli, A., Gabetta, G., Lumachi, A., Fini, L. & Parmigiani, F. Multiphoton electron emission from Cu and W: an angle-resolved study. *Phys. Rev. B* **54**, 6031–6034 (1996).
12. Bormann, R., Gulde, M., Weismann, A., Yalunin, S. V. & Ropers, C. Tip-enhanced strong-field photoemission. *Phys. Rev. Lett.* **105**, 147601 (2010).
13. Li, C. et al. Carbon nanotubes as an ultrafast emitter with a narrow energy spread at optical frequency. *Adv. Mater.* **29**, 1701580 (2017).
14. Li, H. et al. Coherent electronic wave packet motion in C_{60} controlled by the waveform and polarization of few-cycle laser fields. *Phys. Rev. Lett.* **114**, 123004 (2015).
15. Caruso, G. M., Houdellier, F., Abeilhou, P. & Arbouet, A. Development of an ultrafast electron source based on a cold-field emission gun for ultrafast coherent TEM. *Appl. Phys. Lett.* **111**, 023101 (2017).
16. Mourou, G. & Williamson, S. Picosecond electron diffraction. *Appl. Phys. Lett.* **41**, 44–45 (1982).
17. Kozák, M. et al. Ultrafast scanning electron microscope applied for studying the interaction between free electrons and optical near-fields of periodic nanostructures. *J. Appl. Phys.* **124**, 023104 (2018).
18. Tafel, A., Meier, S., Ristein, J. & Hommelhoff, P. Femtosecond laser-induced electron emission from nanodiamond-coated tungsten needle tips. *Phys. Rev. Lett.* **123**, 146802 (2019).
19. Liu, W.-T. et al. Nonlinear broadband photoluminescence of graphene induced by femtosecond laser irradiation. *Phys. Rev. B* **82**, 081408 (2010).
20. Lui, C. H., Mak, K. F., Shan, J. & Heinz, T. F. Ultrafast photoluminescence from graphene. *Phys. Rev. Lett.* **105**, 127404 (2010).
21. Li, T. et al. Femtosecond population inversion and stimulated emission of dense Dirac fermions in graphene. *Phys. Rev. Lett.* **108**, 167401 (2012).
22. Johannsen, J. C. et al. Direct view of hot carrier dynamics in graphene. *Phys. Rev. Lett.* **111**, 027403 (2013).
23. Kim, L., Kim, S., Jha, P. K., Brar, V. W. & Atwater, H. A. Mid-infrared radiative emission from bright hot plasmons in graphene. *Nat. Mater.* **20**, 805–811 (2021).
24. Chen, Y., Li, Y., Zhao, Y., Zhou, H. & Zhu, H. Highly efficient hot electron harvesting from graphene before electron-hole thermalization. *Sci. Adv.* **5**, eaax9958 (2019).
25. Mics, Z. et al. Thermodynamic picture of ultrafast charge transport in graphene. *Nat. Commun.* **6**, 7655 (2015).
26. Massicotte, M. et al. Photo-thermionic effect in vertical graphene heterostructures. *Nat. Commun.* **7**, 12174 (2016).
27. Ma, Q. et al. Tuning ultrafast electron thermalization pathways in a van der Waals heterostructure. *Nat. Phys.* **12**, 455–459 (2016).
28. Sun, D. et al. Ultrafast hot-carrier-dominated photocurrent in graphene. *Nat. Nanotechnol.* **7**, 114–118 (2012).
29. Graham, M. W., Shi, S.-F., Ralph, D. C., Park, J. & McEuen, P. L. Photocurrent measurements of supercollision cooling in graphene. *Nat. Phys.* **9**, 103–108 (2013).
30. Tielrooij, K. J. et al. Generation of photovoltage in graphene on a femtosecond timescale through efficient carrier heating. *Nat. Nanotechnol.* **10**, 437–443 (2015).
31. Yu, R., Guo, Q., Xia, F. & García de Abajo, F. J. Photothermal engineering of graphene plasmons. *Phys. Rev. Lett.* **121**, 057404 (2018).
32. Hafez, H. A. et al. Extremely efficient terahertz high-harmonic generation in graphene by hot Dirac fermions. *Nature* **561**, 507–511 (2018).
33. Tan, S., Argondizzo, A., Wang, C., Cui, X. & Petek, H. Ultrafast multiphoton thermionic photoemission from graphite. *Phys. Rev. X* **7**, 011004 (2017).

34. Wu, G., Wei, X., Gao, S., Chen, Q. & Peng, L. Tunable graphene micro-emitters with fast temporal response and controllable electron emission. *Nat. Commun.* **7**, 11513 (2016).
35. Rezaeifar, F., Ahsan, R., Lin, Q., Chae, H. U. & Kapadia, R. Hot-electron emission processes in waveguide-integrated graphene. *Nat. Photon.* **13**, 843–848 (2019).
36. Keramati, S., Passian, A., Khullar, V. & Batelaan, H. Photofield electron emission from an optical fiber nanotip. *Appl. Phys. Lett.* **117**, 061102 (2020).
37. Căsăndruc, A., Bücker, R., Kassier, G. & Miller, R. J. D. Optical fiber-based photocathode. *Appl. Phys. Lett.* **109**, 091105 (2016).
38. Longo, R. T. A study of thermionic emitters in the regime of practical operation. In *1980 International Electron Devices Meeting* 467–470 https://doi.org/10.1109/IEDM.1980.189868 (1980).
39. Fowler, R. H. & Nordheim, L. Electron emission in intense electric fields. *Proc. R. Soc. Lond. A* **119**, 173–181 (1928).
40. Kampfrath, T., Perfetti, L., Schapper, F., Frischkorn, C. & Wolf, M. Strongly coupled optical phonons in the ultrafast dynamics of the electronic energy and current relaxation in graphite. *Phys. Rev. Lett.* **95**, 187403 (2005).
41. Piscanec, S., Lazzeri, M., Mauri, F., Ferrari, A. C. & Robertson, J. Kohn anomalies and electron-phonon interactions in graphite. *Phys. Rev. Lett.* **93**, 185503 (2004).
42. Yanagisawa, H. et al. Delayed electron emission in strong-field driven tunnelling from a metallic nanotip in the multi-electron regime. *Sci. Rep.* **6**, 35877 (2016).
43. Cheng-Wei Huang, W., Becker, M., Beck, J. & Batelaan, H. Two-color multiphoton emission from nanotips. *N. J. Phys.* **19**, 023011 (2017).

Acknowledgements

This work was supported by National Natural Science Foundation of China (12427806 (K.H.L.), 52025023 (K.H.L.), 51991342 (K.H.L.), 12422406 (H.H.), 12374167 (H.H.), 52102044 (X.Z.) and 52372046 (X.Z.)), the National Key R&D Program of China (2022YFA1403504 (K.H.L.) and 2021YFA1400201 (H.H.)), Guangdong Major Project of Basic and Applied Basic Research (2021B0301030002 (K.H.L.)), the Strategic Priority Research Program of Chinese Academy of Sciences (XDB33000000 (K.H.L.)), and the New Cornerstone Science Foundation through the XPLORER PRIZE (K.H.L.).

Author contributions

K.H.L., H.H., Q.D., and D.Y. supervised the project. K.H.L., H.H., and X.Z. conceived the experiments. G.Y., X.Z., and K.F.L. performed the electrical and optical measurements. G.Y., K.F.L., H.L., and Y.Y. prepared the optical fiber-integrated graphene device. G.Y. performed the ultrafast SEM measurements. G.Y. calculated the hot-electron evolution in graphene. G.Y. and H.L. prepared the on-chip device. Chang Liu and J.Y. suggested the optical experiments. X.F. suggested the ultrafast SEM measurements. Z.W. suggested the electron emission property measurements. K.C. and Chi Li suggested the energy spread measurements. All the authors discussed and contributed to writing the paper.

Competing interests

The authors declare no competing interests.

Additional information

Supplementary information The online version contains supplementary material available at https://doi.org/10.1038/s41467-025-60915-x.

Correspondence and requests for materials should be addressed to Hao Hong, Qing Dai, Dapeng Yu or Kaihui Liu.

Peer review information *Nature Communications* thanks Herman Batelaan and the other anonymous reviewers for their contribution to the peer review of this work. A peer review file is available.